Separation and Purification Technology 271 (2021) 118839

Contents lists available at ScienceDirect

Separation and Purification Technology

journal homepage: www.elsevier.com/locate/seppur

Carbon dioxide capture with aqueous amino acids: Mechanistic study of amino acid regeneration by guanidine crystallization and process intensification

Abishek Kasturi [a,b], Jorge Gabitto [c,*], Costas Tsouris [a,b,*], Radu Custelcean [a,*]

[a] Oak Ridge National Laboratory, P.O. Box 2008, Oak Ridge, TN 37831, United States
[b] School of Civil and Environmental Engineering, Georgia Institute of Technology, United States
[c] Department of Chemical Engineering, Prairie View A&M University, United States

ARTICLE INFO

Keywords:
CO_2 capture
Amino acids
Guanidine crystallization
Process intensification

ABSTRACT

CO_2 capture from powerplant-generated flue gas via a phase-changing process involving absorption with aqueous amino acids (e.g., glycine or sarcosine) and bicarbonate crystallization with bis-iminoguanidines (e.g., glyoxal-bis-iminoguanidine or GBIG) is investigated in this paper. This process is of high interest due to its potential to decrease the energy penalty for CO_2 capture by significantly reducing the solvent regeneration energy typically associated with aqueous amine solvents. A critical step in the proposed CO_2 capture mechanism is the regeneration of the amino acid by removal of protons and bicarbonate ions from solution through crystallization of $GBIGH_2^{2+}$ bicarbonate salt. Here, we investigated the thermodynamics and kinetics of glycine regeneration by crystallization of $GBIGH_2^{2+}(HCO_3^-)_2(H_2O)_2$. A theoretical model was developed and compared to experimental data to simulate and predict the glycine regeneration and determine its reaction mechanism. This combined experimental and theoretical study led to the conclusion that, while the $GBIGH_2^{2+}$ bicarbonate crystallization step provides most of the thermodynamic driving force for the glycine regeneration, the rate-limiting step is the protonation of GBIG prior to crystallization. The CO_2 loading and amino acid regeneration steps were combined into a single, intensified process using a bubble column reactor. The CO_2 loading capacity of GBIG was experimentally determined to be roughly 1.36 mol CO_2 per mol GBIG. These results provide the fundamental basis for developing an effective carbon capture technology with phase-changing amino acid/guanidine absorbents.

1. Introduction

Major reductions in anthropogenic CO_2 emissions will be necessary to slowdown the effects of climate change [1–3]. The most common carbon capture technologies based on adsorption, membrane-based separations, and absorption [4–8], suffer from several limitations. Physical adsorbents are hindered by limited capacities at low CO_2 pressures and the presence of water vapor and other impurities in the gas stream [6]. Membrane-based technologies are hampered by membrane wetting, limited long term stability, and the low selectivity in the presence of other gasses in the gas stream [5]. Most solvents suffer from a combination of high toxicity, high regeneration energy, and a narrow range of operable temperature conditions [7,9,10].

Chemical absorption can be an energy-efficient process if the regeneration of the solvent can be optimized. Aqueous amino acid salts (e.g., potassium glycinate or potassium sarcosinate) have been recently proposed as superior alternatives to conventional amine solvents based on their higher loading capacities, faster CO_2 absorption kinetics, lower volatility and corrosivity, and greater chemical stabilities [11,12]. Amino acids exist in three forms: deprotonated (basic), neutral (zwitterionic), and protonated (acidic), depending on the solution pH. The speciation of glycine and sarcosine is illustrated in Fig. 1. The reaction rate of deprotonated amino acids with CO_2 is several orders of magnitude higher than that of neutral and protonated amino acids [13]. Thus, it is important to be able to regenerate the deprotonated forms of the amino acids effectively and efficiently. Like amines, deprotonated amino acids react with CO_2 to form carbamates. The carbamates then hydrolyze to form bicarbonate anions. CO_2-loaded amino acid solution can be regenerated through heating, which desorbs the CO_2 and restores the basic form of the amino acid. This process, however, is energy intensive,

* Corresponding authors.
E-mail addresses: jfgabitto@pvamu.edu (J. Gabitto), tsourisc@ornl.gov (C. Tsouris), custelceanr@ornl.gov (R. Custelcean).

https://doi.org/10.1016/j.seppur.2021.118839
Received 31 December 2020; Received in revised form 11 March 2021; Accepted 3 April 2021
Available online 30 April 2021

and, over multiple cycles, can chemically degrade the amino acid. An alternative process has been recently proposed, involving regeneration of the amino acid via mineralization of CO_2 with CaO to produce $CaCO_3$ [14,15]. While more energy efficient than conventional regeneration based on heating, the mineralization process is difficult to reverse, as the CO_2 release from $CaCO_3$ requires very high temperatures of about 900 °C. This calcium looping technology has the potential for capturing CO_2 in cement plants as the CaO-rich purge from the calciner can be used to replace a sizable fraction of the $CaCO_3$ used as feedstock [16].

This work examines CO_2 capture by a phase-changing process involving chemical absorption with aqueous amino acid solvents, such as glycine or sarcosine, followed by (bi)carbonate crystallization with guanidine compounds, such as bis-iminoguanidines (BIGs) [17–19]. This process consists of three steps: (1) CO_2 absorption with aqueous amino acids, yielding the corresponding (bi)carbonate salts (together with a small amount of carbamate); (2) crystallization of the (bi)carbonate anions with a BIG solid, which regenerates the amino acid; and (3) solid-state CO_2 release from the (bi)carbonate crystals and regeneration of the BIG. The overall CO_2 separation cycle is depicted in Fig. 2, using glycine and glyoxal-bis(iminoguanidine) (GBIG) as representative amino acid and BIG compounds. Like other phase-changing processes for CO_2 capture [20,21], the amino acid/BIG process combines the benefits of aqueous solvents such as fast CO_2 absorption rates, easy handling, and scalability with the advantages of solid-state sorbents, such as lower regeneration energy and temperature and minimal sorbent loss through evaporation. Furthermore, the precipitation of GBIG carbonate allows for easy separation and regeneration of the CO_2 loaded solvent. For the particular case of glycine/GBIG, the regeneration energy was found to be 24% and 40% lower than the regeneration energies of benchmark aqueous absorbents monoethanolamine (MEA) and sodium glycinate, respectively [19]. The significantly reduced energy requirement for the phase-changing glycine/GBIG process is mostly due to avoiding heating the aqueous amino acid solution, as only the precipitated $GBIGH_2^{2+}(HCO_3^-)_2$ $(H_2O)_2$ solid needs to be heated to release the CO_2.

The critical step in the CO_2 separation cycle with glycine/GBIG is the precipitation of the $GBIGH_2^{2+}(HCO_3^-)_2(H_2O)_2$ solid, as this reaction not only removes the CO_2 from solution but also regenerates the deprotonated form of the amino acid, which can be recycled. The main objective of this paper is to investigate in detail the glycine regeneration with GBIG, as an important step toward developing an energy-efficient CO_2 capture technology. Here, we report our findings regarding the thermodynamics and kinetics of glycine regeneration with GBIG. The experimental data are analyzed with the help of a theoretical model developed as part of this study, leading to a proposed mechanism of amino acid regeneration with GBIG. To improve the efficiency of the capture mechanism, a three-phase bubble column reactor was employed to combine CO_2 loading and deprotonated amino acid regeneration into an intensified process. A bubble column was used since it provides good mixing and high interfacial surface area for mass and heat transfer. The absorption capacity of this intensified process was experimentally determined through a reaction with gaseous CO_2, aqueous KOH-amino-

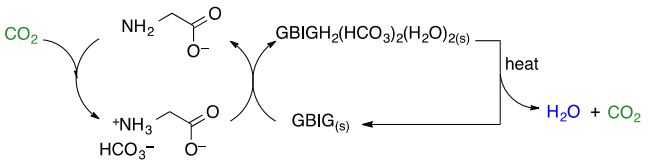

Fig. 2. Overall process scheme for CO_2 capture using glycine and GBIG [19].

acid solution, and solid GBIG. Overall, this study provides the fundamental basis for developing an effective carbon capture technology with phase-changing amino acid/guanidine absorbents [22]. The novelty of this study is that it identifies the process rate-limiting step, and shows how process intensification can be achieved by combining CO_2 loading and deprotonated amino acid regeneration into a single unit operation.

2. Materials and methods

2.1. Chemicals

All the chemicals used in this study, except for GBIG, were directly purchased from vendors and were used without any further purification. GBIG was synthesized in-house as described in a published procedure [23]. Glycine and sarcosine (>99% purity) were purchased from Sigma Aldrich, Milwaukee. Potassium bicarbonate (>99% purity) was purchased from Fischer Scientific. Simulated flue gas (12.8% CO_2 and 87.2% N_2) was purchased from Airgas. GBIG was regenerated by heating the vacuum-dried precipitate at 100 °C for 2 h.

2.2. Equipment

A jacketed vessel with temperature control was used to run the kinetics experiments. The variable-temperature thermodynamic measurements were conducted in a Heratherm incubation chamber, using syringe filters (0.22 μm) from Thermo Fisher to draw the samples for analysis. The syringe filters helped stop the reaction from progressing by separating the GBIG from the liquid phase. Dionex ICS-5000 + ion chromatography system with an inline eluent generator was used for ion chromatography (IC) measurements. Solution pH measurements were done with a Thermo Fischer's Accumet pH meter. A bubble column reactor made from pyrex glass with an internal diameter of 3 in. and a height of 36 in. was used in the three-phase experiments. A bubble diffuser made from a 0.25-in. outside-diameter porous polymer tube was located at the bottom of the column to disperse the flue gas in the liquid. The solvent was pumped from the top of the column, and the exit liquid at the bottom was recycled using a Cole Parmer Masterflex diaphragm pump. The exiting liquid was delivered through a pH probe and sampled before being recycled. Exit pH and conductivity were measured using the Acumet pH meter 50. The exit gas at the top was passed through a CM-0003 CO_2 meter for exit CO_2 concentration readings before being purged.

Amino Acid	Structure		
	Acidic	Zwitterionic	Basic
Glycine	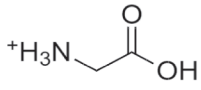	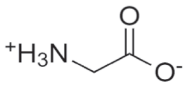	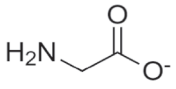
Sarcosine	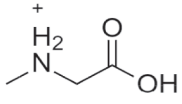	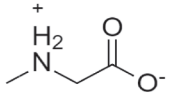	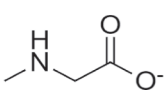

Fig. 1. Speciation of glycine and sarcosine.

3. Experimental methods

3.1. Thermodynamic measurements

The thermodynamic behavior of the amino acid (AA) regeneration reaction was analyzed based on Eq. (1), according to a previously published method [18].

$$2HCO_3^-(aq)+2AA\text{-}H_{(aq)}+GBIG_{(s)}\leftrightarrow\left[GBIGH_2^{2+}\left(HCO_3^-\right)_2(H_2O)_2\right]_{(s)}+2AA^-_{(aq)} \quad (1)$$

Samples of 20-mL solution containing 0.3 M $KHCO_3$, 0.5 M glycine, and 0.25 M equivalent GBIG were prepared and stirred overnight on a rotating wheel in the incubator. The pH and the carbonate concentration of the equilibrated solutions were measured via a pH probe and ion chromatography, respectively. The samples were passed through a syringe filter before being analyzed. The equilibrium reactions were performed at 5 different temperatures: 15, 20, 22, 25, and 30 °C. This process was repeated.

Potassium bicarbonate was used to reduce the number of phases involved in the thermodynamics and kinetics studies. The overall capture process consists of three phases – the gaseous flue gas, the aqueous KOH-amino acid solution, and the solid GBIG. The regeneration of the amino acid takes place in the aqueous phase, with dissolved CO_2 in the form of HCO_3^-. The speciation of the amino acid and dissolved CO_2 can be calculated using pH and bicarbonate concentration. Ion chromatography was used to determine the total carbonate concentration, which is the sum of $[CO_3]^{2-}$ and $[HCO_3]^-$. The concentration of HCO_3^- can then be calculated using the relevant equilibrium constant and pH values.

The equilibrium constant for the regeneration reaction (K_{reg}) was calculated using Eq. (2).

$$Kreg=\frac{\gamma^2_{AA^-}[AA^-]^2}{\gamma^2_{AA-H}[AA-H]^2\gamma^2_{HCO_3^-}\left[HCO_3^-\right]^2} \quad (2)$$

Since both the deprotonated amino acid (AA^-) and the bicarbonate ion are single-charged anions, their respective activities can be assumed to be equal and cancel each other. The concentrations and activities of GBIG and $GBIGH_2^{2+}(HCO_3)_2$ do not appear in the equilibrium constant equation since the two species are solids. Thus, to determine the equilibrium constant for the reaction, the values of the following species are required: $[AA^-]$, [AA-H], $[HCO_3^-]$, $\gamma_{AA\text{-}H}$ [24,25].

The speciations of bicarbonate and the amino acids used can be calculated from their respective K_a values and the measured pH of the solution, using Eqs. (3) and (4). Once the equilibrium constants were calculated for each temperature, the reaction enthalpy was determined from the van't Hoff plot.

$$HCO_3^- \rightleftharpoons CO_3^{2-}+H^+ \quad (3)$$

$$\frac{K_{a_{HCO_3}}}{[H^+]}=\frac{\left[CO_3^{2-}\right]}{\left[HCO_3^-\right]} \quad (4)$$

$$Gly \rightleftharpoons Gly^- + H^+ \quad (5)$$

$$\frac{K_{a_{gly}}}{[H^+]}=\frac{[Gly^-]}{[Gly]} \quad (6)$$

3.2. Kinetic measurements

The kinetics of the amino acid regeneration reaction (Eq. (1)) were measured using initial concentrations of reactants as summarized in Table 1.

A 100-mL volume of solution containing $KHCO_3$ and glycine was prepared and left to equilibrate at 25 °C in the jacketed stirred reactor. Once the temperature and pH of the solution equilibrated, solid GBIG was added to the solution and the pH was continuously monitored. 0.25 mL samples were drawn through a syringe filter every 30 s for the first five minutes and every minute thereafter. The filtered samples were analyzed for their total carbonate concentration by ion chromatography. The setup of the thermodynamics and kinetics experiments is shown in Fig. 3a.

Table 1
Concentrations (M) of reagents used in the kinetics experiments.

Experiment #	$[KHCO_3]$	[Glycine]	[GBIG]
1	0.30	0.50	0.25
2	0.03	0.05	0.025
3	0.05	0.05	0.025
4	0.1	0.05	0.025
5	0.1	0.1	0.025
6	0.1	0.5	0.025

3.3. Three phase system

The CO_2 loading of a three-phase system consisting of 3 L of 1 M KOH, 1 M sarcosine, 0.5 M GBIG, and simulated flue gas with a flow rate of 4 L min^{-1} was studied in a bubble column reactor shown in Fig. 3b. The liquid at the bottom of the bubble column reactor was drawn for sampling every 2 min for the first 20 min and every 5 min thereafter. These samples were then analyzed for their total carbonate concentration using ion chromatography and pH. A CO_2 meter was used to measure the concentration of the exiting gas at the top of the column every 5 s. The total amount of moles of CO_2 absorbed was calculated by finding the area underneath the absorption profile. The three-phase system was studied using sarcosine instead of glycine after it was determined that sarcosine was more stable than glycine if impurities were present during thermal regeneration.

3.4. Theoretical section

In order to study amino acid regeneration with BIG compounds, we propose a set of complex chemical reactions involving BIG species, amino acid species, the aqueous solvent, and the carbonated compounds. In the case of a typical amino acid, such as glycine ($NH_2CH_2CO_2H$), and a typical BIG compound, such as GBIG, we propose the following set of reactions:

$$GBIG(s) \overset{K_{sp}}{\Leftrightarrow} GBIG(aq) \quad (7)$$

$$GBIG(aq)+2GLYH(aq) \overset{K_2}{\Leftrightarrow} GBIGH_2^{2+}(aq)+2GLY^-(aq) \quad (8)$$

$$GBIGH_2^{2+}(aq)+2HCO_3^-(aq)+2H_2O \overset{K_3}{\Leftrightarrow} GBIGH_2^{2+}\left(HCO_3^-\right)_2(H_2O)_2(s) \quad (9)$$

$$HCO_3^-(aq)+GLY^-(aq) \overset{K_4}{\Leftrightarrow} GLY^-(CO_2^-)(aq)+H_2O \quad (10)$$

$$GLY^-(aq)+H^+ \overset{K_5}{\Leftrightarrow} GLYH(aq) \quad (11)$$

$$HCO_3^-(aq)+OH^- \overset{K_6}{\Leftrightarrow} CO_3^{2-}(aq)+H_2O \quad (12)$$

$$H^+ + GLY^-\left(CO_2^-\right)(aq) \overset{K_7}{\Leftrightarrow} GLY^-(CO_2H)(aq) \quad (13)$$

$$H_2O \overset{K_w}{\Leftrightarrow} H^+ + OH^- \quad (14)$$

$$HCO_3^-(aq)+H_2O \overset{K_8}{\Leftrightarrow} H_2CO_3(aq)+OH^- \quad (15)$$

Eq. (7) represents the dissolution of solid GBIG. Eq. (8) represents the proton transfer from glycine to GBIG to regenerate the anionic form of glycine and form the dicationic form of GBIG, which then precipitates

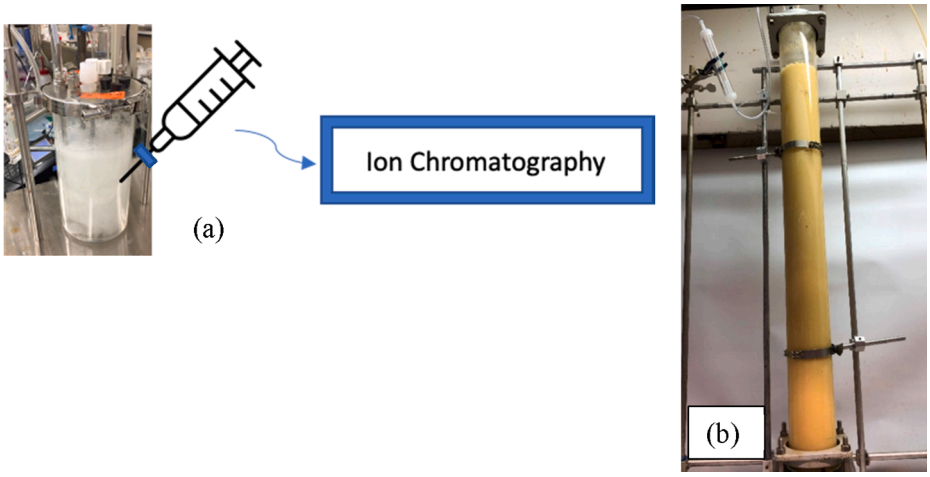

Fig. 3. (a). Setup of thermodynamics and kinetics experiments in a 1-L reactor. **(b)** 3-L, 3-phase column reactor used for process intensification.

with bicarbonate anions and water, according to Eq. (9) [17]. The bicarbonate anions also react with the alkaline form of glycine to produce a carbamate compound, according to Eq. (10). The carbamate compound is at equilibrium with the protonated carbamic acid form through Eq. (13). The neutral form the amino acid (GLYH) is at equilibrium with the alkaline form (GLY^-) through Eq. (11). The bicarbonate ion is at equilibrium with carbonic acid and carbonate ions following Eqs. (12) and (15). The net reaction rates for Eqs. (7)–(15) can be generally written as:

$$R_i = r_{if} - r_{ir} \tag{16}$$

where Ri is the reaction rate of the i-equation and r_{if} and r_{ir} are the forward and reverse reaction rates of the i-reaction, respectively.

3.5. Model derivation

Inspection of Eqs. (7)–(15) leads us to propose the following assumptions:

I. The reaction rates of Eqs. (11)–(15), corresponding to solution acid-base reactions, are very fast and, therefore, the chemical compounds participating in these reactions are at equilibrium. Eq. (7) corresponding to GBIG dissolution is also assumed to be fast based on experimental observations (see below).
II. The reactions given by Eqs. (8), (9), and (10) are relatively slow and, thus, these reactions control the overall rate of the reaction system.

In making these assumptions, we took into account the following observations:

III. Some GBIG dissolution experiments (not included here), showed that reaction (7) is very fast (equilibrium is reached within 35 s) and that [GBIG(aq)] concentrations can be considered equilibrium values.
IV. Reaction (10) has been studied for the similar amino acid sarcosine, and kinetic parameters are available in the literature [17].
V. Equilibrium constants for reactions (8) and (9) have been measured in literature, but there are no values reported of the specific kinetic rate constants [17].

The assumptions and observations I to V lead to the following set of equations:

$$K_{sp} = [GBIG(aq)] \tag{17}$$

$$K_5 = \frac{[GLYH]}{[GLY^-][H^+]} \tag{18}$$

$$K_6 = \frac{[CO_3{}^{2-}]}{[HCO_3{}^-][OH^-]} \tag{19}$$

$$K_7 = \frac{[GLY^-(CO_2H)]}{[GLY^-(CO_2^-)][H^+]} \tag{20}$$

$$K_w = [H^+][OH^-] \tag{21}$$

$$K_8 = \frac{[H_2CO_3][OH^-]}{[HCO_3{}^-]} \tag{22}$$

The concentrations of the cationic guanidine compound ($GBIGH_2^{2+}$), the carbamate $[GLY^-(CO_2^-)]$, and the precipitate $[GBIGH_2^{2+}(HCO_3^-)_2(H_2O)_2]$ are calculated using the following differential equations:

$$\frac{\partial[GLY^-(CO_2^-)]}{\partial t} = k_{4f}\left\{[HCO_3{}^-][GLY^-] - \frac{1}{K_4}[GLY^-(CO_2^-)]\right\} - k_{7f}\{[H^+][GLY^-(CO_2^-)] - \frac{1}{K_7}[GLY^-(CO_2H)]\} \tag{23}$$

$$\frac{\partial[GBIGH_2^{2+}]}{\partial t} = k_{2f}\{[GBIG(aq.)][GLYH]^2 - \frac{1}{K_2}[GBIGH_2^{2+}][GLY^-]^2\} - k_{3f}\{[GBIGH_2^{2+}][HCO_3{}^-]^2 - \frac{1}{K_3}\} \tag{24}$$

$$\frac{\partial[GBIGH_2(HCO_3^-)_2(H_2O)_2]}{\partial t} = k_{3f}\{[GBIGH_2^{2+}][HCO_3{}^-]^2 - \frac{1}{K_3}\} \tag{25}$$

The concentration of the precipitate appearing in Eq. (25) represents the amount of ions disappearing from the liquid phase, as the

concentration of a solid does not have physical meaning for this system. In order to close the system of algebraic and differential equations, mass balances for the amounts of carbon and amino acid, plus a charge balance, are used:

3.6. Carbon mass balance

$$[HCO_3^-]_o = [HCO_3^-] + [CO_3^{2-}] + [GLY^-(CO_2^-)] + [GLY^-(CO_2H)] + 2[GBIGH_2^{2+}(HCO_3^-)_2(H_2O)_2] \quad (26)$$

Here, $[HCO_3^-]_o$ is the initial concentration of the bicarbonate ion.

3.7. Amino acid mass balance

$$[GLY^-]_o = [GLY^-] + [GLYH] + [GLY^-(CO_2^-)] + [GLY^-(CO_2H)] \quad (27)$$

3.8. Charge balance

$$[HCO_3^-] + 2[CO_3^{2-}] + 2[GLY^-(CO_2^-)] + [GLY^-(CO_2H)] + [GLY^-] + [OH^-] = [K^+]_o + [H^+] + 2[GBIGH_2^{2+}] \quad (28)$$

Here, $[K^+]_o$ represents the initial concentration of a monovalent cation accompanying the bicarbonate ion.

3.9. Model implementation

The combined system of algebraic and differential equations given by Eqs. (16)–(28) was solved numerically. The ordinary differential Eqs. (23)–(25) were solved numerically for every time step of the calculations using a second order finite differences method. The calculated values were introduced into an algebraically derived equation, Eq. (29), that calculates the $[OH^-]$ and, consequently, pH of the system at that particular time step. The calculated value of the pH allows calculation of the concentrations of all chemical species present in the system. This procedure was implemented into a FORTRAN computer code. The computer code was validated by calculation of the pH of specific cases of the chemical system used and comparison with known values obtained from literature or calculated by other methods. An example is the case, where $[HCO_3^-]_o = 0.1$ M and there is neither amino acid nor guanidine compound present. In this particular case, using the procedure reported by Stumm and Morgan [27], the calculated pH value is 8.31. The calculated value using the procedure reported in this work is 8.303.

$$\frac{C_o - 2GPP - [GLY^-(CO_2^-)](1 + K_7K_w/[OH^-])}{(1 + K_6[OH^-] + \frac{K_8}{[OH^-]})}(1 + 2K_6[OH^-]) + [GLY^-(CO_2^-)](2 + K_7K_w/[OH^-]) + [OH^-] + \frac{C_1 - [GLY^-(CO_2^-)](1 + K_7K_w/[OH^-])}{(1 + K_5K_w/[OH^-])} = C_o + \frac{K_w}{[OH^-]} + 2[GBIGH_2^{2+}] \quad (29)$$

Here, $C_o = [HCO_3^-]_o$, $C_1 = [K^+]_o + 2[GBIGH_2^{2+}]$, and GPP is the 'virtual' concentration of the guanidine precipitate.

Table 2
Equilibrium constant values for the glycine regeneration reaction with GBIG.

Temperature (°C)	Log K_{reg}
15	2.58
20	2.41
22	2.36
25	2.09
30	2.03

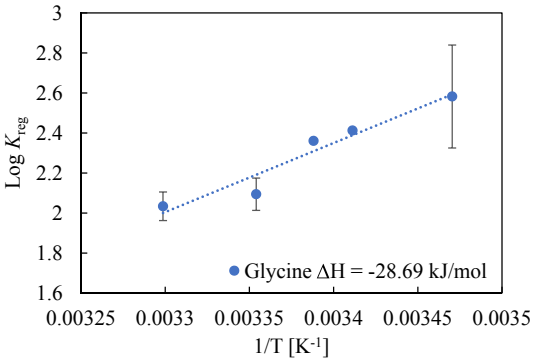

Fig. 4. van't Hoff plot for the glycine regeneration reaction with GBIG.

4. Results and discussion

4.1. Thermodynamics

The goal of the thermodynamics measurements was to determine the equilibrium constants at different temperatures and the enthalpy of reaction for the glycine regeneration by GBIG (Eq. (1)). The obtained K_{reg} values, calculated with Eq. (2), are listed in Table 2. The regeneration reaction is thermodynamically favorable at all measured temperatures, with logK_{reg} ranging between 2.03 and 2.58.

The van't Hoff plot for the glycine regeneration reaction is shown in Fig. 4. The enthalpy of reaction, determined from the slope of the van't Hoff plot, is –28.69 kJ/mol. Thus, the glycine regeneration by crystallization with GBIG is favorable and exothermic. For comparison, the regeneration of glycine by conventional heating is endothermic, with a reported reaction enthalpy of 69 kJ/mol [26].

4.2. Kinetics

We used a combination of experimental data and simulations results to determine the controlling steps in the complex reaction mechanism proposed. In the subsections bellow, we summarize our results and draw the relevant conclusions. The initial concentrations of the reagents used in kinetics experiments are shown in Table 1.

The goal of the kinetic experiments was to gain insight into the reaction mechanism of glycine regeneration with GBIG. The two experimental variables determined in this work were the total carbonate ion concentration, $[HCO_3^-] + [CO_3^{2-}]$, and the pH. The individual concentrations of the bicarbonate and carbonate ions were determined using Eq. (19). The results of varying the initial reactant concentrations

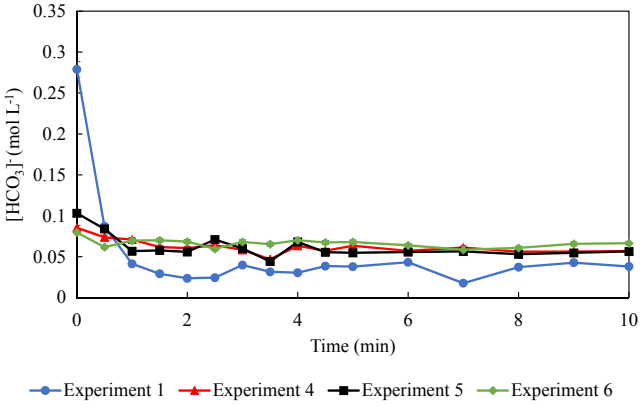

Fig. 5. Kinetic results showing the change in the total bicarbonate concentration in solution as a function of time, for different initial reactant concentrations (see Table 1).

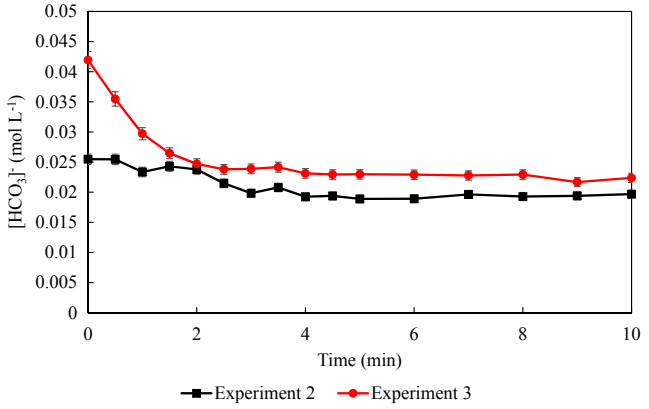

Fig. 6. Kinetic results showing the change in the total bicarbonate concentration in solution as a function of time, for different initial reactant concentrations (see Table 1).

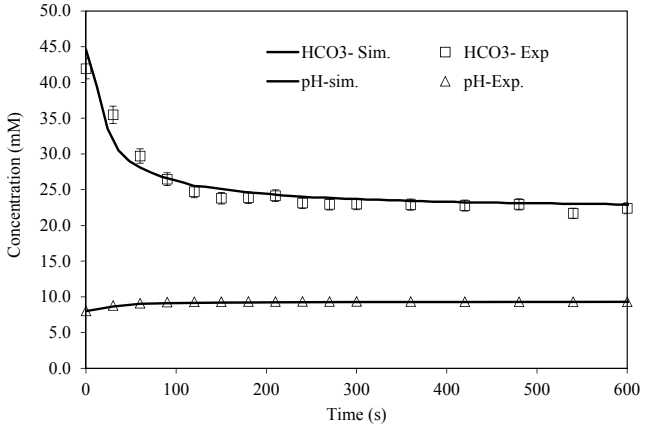

Fig. 7. Comparison of simulated bicarbonate and pH values with the experimental data for Experiment 3.

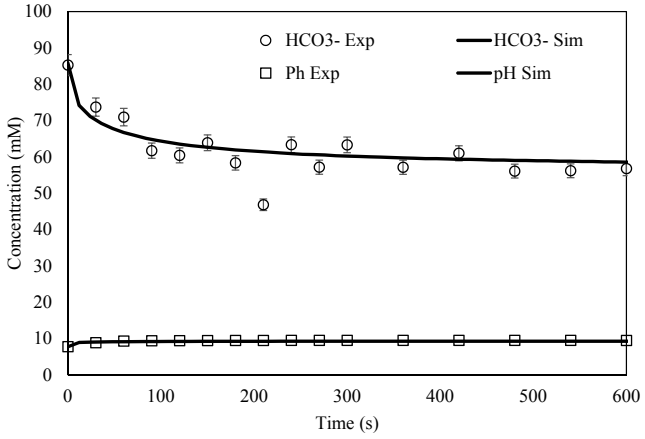

Fig. 8. Comparison of time variation of bicarbonate and pH simulation results and experimental data for Experiment 4.

of bicarbonate and amino acid (as per Table 1) are presented in Figs. 5 and 6.

The purpose of the changes in initial reactant concentrations was to find the optimum set of parameters that yielded the largest amount of experimental data with minimal experimental errors. One particular challenge was to slow down the overall regeneration reaction in order to maximize the number of experimental observations in the initial phase of the reaction (first 60 s), before reaching equilibrium. This had to be balanced against the requirement to have a large enough decrease in the carbonate concentration at equilibrium to minimize the experimental uncertainties. Despite efforts to slow down the reaction by diluting the starting concentrations of the reactants, the results presented in Figs. 5 and 6 show that the reaction is mostly completed within the first 30–60 s under all conditions. After the initial fast reaction, a steady-state regime is achieved, corresponding to the equilibrium point of the regeneration reaction. Experiments 3 and 4, which provided the most reliable data, were selected for further theoretical analysis.

5. Simulation results

In all simulation scenarios, we assumed that reasonable agreement between experimental data and simulation results was an indication that the proposed kinetic mechanism was acceptable. Assumptions (I) and (II) imply that reactions (8) and (9) control the overall rate of the complex kinetic mechanism. Assumption (II) implies the kinetic parameters that determine the rate of the whole process are the forward specific rate constants and the equilibrium constants of Eqs. (8) and (9), k_{f2}, K_2, k_{f3}, K_3. The two equilibrium constants have been estimated in the open literature but, presently, there are no data related to the two forward specific rate constants. In order to study the reaction system, we conducted many different simulation runs trying to fit the calculated results using the four aforementioned kinetic parameters to the experimental data [17]. The initial simulations with the values of the two equilibrium constants determined from the literature kept fixed did not lead to a good fitting; therefore, we tried the same procedure, but varying all four kinetic parameters. Several simulation runs led to the following observations:

1) The plotted curve can be divided in two parts: fast concentration changes in the early stage of the reaction, followed by a steady-state part.
2) The value of the forward specific reaction rate constant for Eq. (8), k_{f2}, determines the time needed for the system to reach the steady-state equilibrium.
3) The values of the equilibrium constants K_2 and K_3 determine the position of the steady-state equilibrium point.
4) Big chances in the value of Eq. (9) forward specific rate constant, k_{f3}, produce very small changes in the observed response.
5) Big changes in the value of the equilibrium constant of Eq. (9), K_3, produce little change in the predicted response.
6) Small changes in the equilibrium constant for Eq. (8), K_2, produce significant changes in the values of the steady-state part of the curve.

Based upon on the observations (1) to (6), we fitted the simulated results to the experimental data using, k_{f2}, K_2, k_{f3}, as unknown parameters while keeping the equilibrium constant of Eq. (9), K_3, equal to the literature value [17]. Our results are shown in Fig. 7 for Experiment 3 and Fig. 8 for Experiment 4. The symbols represent experimental data, while the lines represent simulated results. The values of the four kinetic parameters used in the simulations are shown in Table 3.

Table 3
Kinetic parameters determined by fitting simulation results to experimental data.

Experiment	k_{f2}	K_2	k_{f3}	K_3
1	2.52E-05	3.10E-05	0.0110	0.54
2	1.50E-05	9.10E-06	0.0082	0.54
3	9.60E-06	3.42E-05	0.00833	0.54
4	2.08E-05	3.25E-05	0.00920	0.54
5	2.10E-05	6.20E-06	0.00820	0.54
6	2.18E-05	3.25E-05	0.00920	0.54
Average:	1.99E-05	2.26E-05	0.00895	0.54

We found very good agreement between simulated results, using the kinetic parameters shown in Table 3 and the experimental data. A similar comparison between simulated results and the experimental data measured in Experiment 4 is shown in Fig. 8.

We can also see that there is very good agreement between experimental data and simulated results calculated using the data shown in Table 3. For the sake of completeness, we fitted all sets of experimental data for the conditions shown in Table 1, even though some of the experimental data sets have higher errors than the sets corresponding to experiments 3 and 4. The values of all determined kinetic parameters are also shown in Table 3. Inspection of the predicted kinetic parameters shows variations of values for different data sets. This discrepancy is attributed to the experimental error involved in different data sets. Average values for all the parameters are also shown in Table 3. As previously mentioned, however, the values corresponding to Experiments 3 and 4 are more reliable than those of the other experimental sets due to smaller experimental errors. Experiments 3 and 4 also showed better agreement between calculated results and experimental data.

Observations (1) to (6) and the discussion of the results shown in Figs. 7 and 8 lead us to conclude that the proposed reaction sequence represents an acceptable picture of the complex kinetic mechanism. The good agreement between simulation results and experimental data seems to support the fact that Eqs. (8) and (9) control the behavior of the whole system. Our simulation results point out to Eq. (8) as the limiting step. Eq. (8) represents the generation of the $GBIGH_2^{2+}$ cation by deprotonation of the amino acid. This conclusion is supported by the important role played by the kinetic parameters of Eq. (8), k_{f2} and K_2. The formation of the $GBIGH_2^{2+}(HCO_3^-)_2(H_2O)_2$ precipitate does not seem to control the rate of the process; therefore, this reaction should be considered faster than the protonation of the GBIG by glycine. This conclusion is supported by the minor role played by the forward specific rate, k_{f3}. However, the value of the equilibrium constant of the precipitate formation reaction (K_3) significantly influences the steady-state equilibrium concentration value.

6. Process intensification experiments

A three-phase gas–liquid-solid system as shown in Fig. 3b was used for simultaneous CO_2 capture and amino acid regeneration into a single, continuous, intensified process. Regeneration studies of solid GBIG bicarbonate indicated that insufficiently washed and dried slurries containing glycine degraded during thermal regeneration and produced ammonia gas, thus, the three-phase system was studied using sarcosine because of sarcosine's greater stability during thermal regeneration. Fig. 9 illustrates the CO_2 loading profile in the three-phase system (top) compared to the two-phase system of CO_2 capture by the amino acid (bottom).

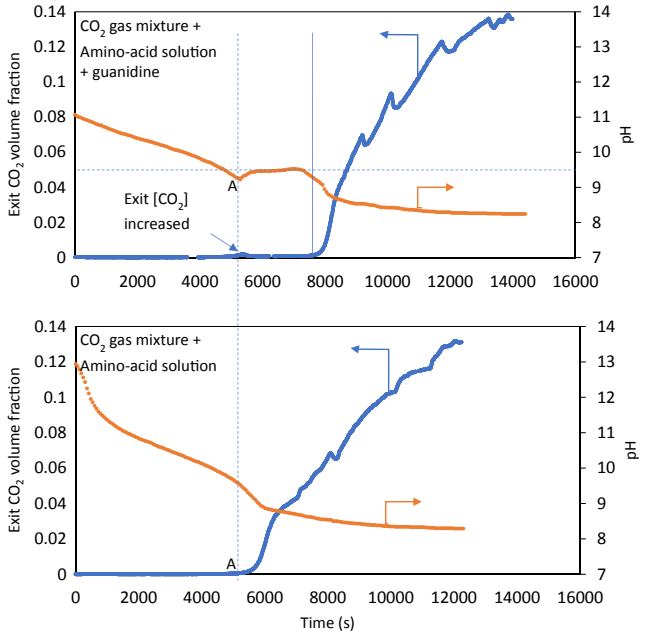

Fig. 9. Comparison of CO_2 loading by the three-phase (gas–liquid-solid) system (top) with the two-phase (gas–liquid) system (bottom).

Identical experimental conditions with respect to flowrates and concentrations were used in the two types of experiments presented in Fig. 9. For the gas–liquid reactor without guanidine, CO_2 breakthrough started at point A. At the same point, for the three-phase system, the exit concentration of CO_2 started increasing, but then the pH stabilized at 9.5 and the CO_2 concentration went back to zero for an extended period of time. The behavior observed in Fig. 9 (top) can be explained as follows. As CO_2 is bubbled through the suspension, the pH starts dropping until it is low enough to protonate the BIG. When that happens, BIG-carbonate starts precipitating, which removes protons from solution. A steady state can be reached when the rate of pH drop from continuously added CO_2 equals the rate of proton removal from solution by crystallization. Eventually the system runs out of GBIG and the pH starts dropping again until the amino acid is saturated with CO_2. This behavior has been reproduced in multiple experiments, and indicates that CO_2 absorption and amino-acid regeneration can occur in a single reactor, leading to process intensification, while the three-phase reactor helps eliminate one processing step, potentially reducing the capital and operating costs of the CO_2 capture process.

By plotting the volume of CO_2 absorbed vs time, we determined the total moles of CO_2 absorbed by calculating the area underneath the absorption profile. Approximately 16.65 L of CO_2 was absorbed, and through the ideal gas law, this volume was translated to roughly 0.68 mol of CO_2 absorbed. The absorption capacity of the GBIG-sarcosine system can thus be estimated and compared with other commonly used solvents or sorbents. The comparison shown in Table 4 demonstrates that the intensified amino acid-guanidine system of this work is very competitive. Diaz et al. indicate in their research that sodium glycinate and sodium prolinate had CO_2 loading capacities of approximately 0.5 mol CO_2 per mol amine, and that the regeneration of deprotonated amino acids can increase the loading capacity of the solvent. Results presented in this paper corroborate these findings by Diaz et al. [27].

7. Conclusions

In this study, the thermodynamics and kinetics of the regeneration of glycine, a typical amino acid solvent used for CO_2 capture, by crystallization with a guanidine compound (GBIG), were investigated in order to propose a plausible reaction mechanism. The regeneration reaction of glycine with GBIG was found to be exothermic, with a measured enthalpy of reaction of –28.7 kJ/mol. This stands in direct contrast with the corresponding endothermic enthalpy of 69 kJ/mol for the thermally-driven regeneration of aqueous glycine solvent.

The kinetics of the system were measured experimentally, and the results were analyzed using a simulation model. The protonation reaction of GBIG by the glycine, and the subsequent crystallization of

Table 4
CO_2 loading of other common CO_2 capture technologies.

Sorbent	Concentration	CO_2 loading (moles CO_2/mol sorbent)
GBIG	0.5 mol L^{-1}	1.36
BTIG[28]	0.01 mol L^{-1}	1.46
Pure aqueous MEA[19]	30 wt%	0.67
MEA/sulfolane [29]	4:5 mol L^{-1}	1.00
BDA/DMCA [30]	3:7 mol L^{-1}	0.70

Note: Solvents in bold phase are phase changing solvents like GBIG.

$GBIGH_2^{2+}(HCO_3^-)_2(H_2O)_2$ were found to be the controlling steps of the overall regeneration process. While the protonation of GBIG was determined to be the rate limiting step in the amino acid regeneration mechanism, the $GBIGH_2^{2+}$ bicarbonate crystallization provides significant thermodynamic driving force for the glycine regeneration.

The performance of an intensified process, where CO_2 from a gas phase is captured by an amino acid in a liquid solution in the presence of GBIG, which serves to in situ regenerate the amino acid, demonstrated CO_2 capture enhancement compared to the same system without GBIG. It was found that 1.36 mol of CO_2 were absorbed per mole of sorbent. This absorption performance is competitive with other solvents currently being investigated. The three-phase system was studied using sarcosine, and the results can be used to generalize the behavior of amino acids in process intensification. However, more work is needed to select combinations of amino acids and guanidine compounds for optimal performance.

The combined experimental measurements and simulation model presented in this work, along with the performance of the three-phase system, will be helpful in future efforts to optimize and scale up this phase-changing CO_2 separation process and ultimately develop an effective carbon capture technology.

Declaration of Competing Interest

The authors declare that they have no known competing financial interests or personal relationships that could have appeared to influence the work reported in this paper.

Acknowledgements

This research was supported by the Seed Money Fund of the Laboratory Directed Research and Development program of the Oak Ridge National Laboratory (ORNL). The experimental thermodynamic and kinetic measurements and analysis by AK and RC, was partially supported by the US Department of Energy, Office of Science, Basic Energy Sciences, Chemical Sciences, Geosciences, and Biosciences Division.

Appendix A. Supplementary material

Supplementary data to this article can be found online at https://doi.org/10.1016/j.seppur.2021.118839.

References

[1] V. Masson-Delmotte, P. Zhai, H.-O. Pörtner, D. Roberts, J. Skea, P.R. Shukla, A. Pirani, W. M.-O., C. Péan, R. Pidcock, S. Connors, J.B.R. Matthews, Y. Chen, X. Zhou, M.I. Gomis,; E. Lonnoy, T. M., M. Tignor, T. Waterfield (Eds.), Global Warming of 1.5°C. An IPCC Special Report on the impacts of global warming of 1.5°C above pre-industrial levels and related global greenhouse gas emission pathways, in the context of strengthening the global response to the threat of climate change, sustainable development, and efforts to eradicate poverty Geneva, 2018.

[2] Ed Dlugokencky, P. T. Trends in Atmospheric Carbon Dioxide https://www.esrl.noaa.gov/gmd/ccgg/trends/global.html.

[3] J. Blunden, D.S. Arndt, State of the climate in 2018, Bull. Am. Meteorol. Soc. 100 (9) (2019) Si-S306.

[4] D. Aaron, C. Tsouris, Separation of CO_2 from flue gas: a review, Sep. Sci. Technol. 40 (1–3) (2005) 321–348.

[5] P. Luis, T. Van Gerven, B. Van der Bruggen, Recent developments in membrane-based technologies for CO_2 capture, Prog. Energy Combust. Sci. 38 (3) (2012) 419–448.

[6] C.-H. Yu, C.-H. Huang, C.-S. Tan, A review of CO_2 capture by absorption and adsorption, Aerosol Air Qual. Res. 12 (5) (2012) 745–769.

[7] Y. Wang, L. Zhao, A. Otto, M. Robinius, D. Stolten, A review of post-combustion CO2 capture technologies from coal-fired power plants, Energy Procedia 114 (2017) 650–665.

[8] M. Fasihi, O. Efimova, C. Breyer, Techno-economic assessment of CO_2 direct air capture plants, J. Cleaner Prod. 224 (2019) 957–980.

[9] R. Notz, H.P. Mangalapally, H. Hasse, Post combustion CO_2 capture by reactive absorption: Pilot plant description and results of systematic studies with MEA, Int. J. Greenhouse Gas Control 6 (2012) 84–112.

[10] E.B. Rinker, S.S. Ashour, O.C. Sandall, Absorption of carbon dioxide into aqueous blends of diethanolamine and methyldiethanolamine, Ind. Eng. Chem. Res. 39 (11) (2000) 4346–4356.

[11] A.M. Shariff, S. M. S., Aqueous amino acid salts and their blends as efficient absorbents for CO2 capture. In: W., B., Ed., Energy Efficient Solvents for CO2 Capture by Gas-Liquid Absorption, Springer, Cham: Green Energy and Technology, 2017, pp 117-151.

[12] V. Sang Sefidi, P. Luis, Advanced amino acid-based technologies for CO_2 capture: a review, Ind. Eng. Chem. Res. 58 (44) (2019) 20181–20194.

[13] D. Guo, H. Thee, C.Y. Tan, J. Chen, W. Fei, S. Kentish, G.W. Stevens, G. da Silva, Amino acids as carbon capture solvents: chemical kinetics and mechanism of the glycine + CO_2 reaction, Energy Fuels 27 (7) (2013) 3898–3904.

[14] M. Liu, G. Gadikota, Single-step, low temperature and integrated CO_2 capture and conversion using sodium glycinate to produce calcium carbonate, Fuel 275 (2020), 117887.

[15] Y. Li, X. Duan, W. Song, L. Ma, J. Jow, Reaction mechanisms of carbon dioxide capture by amino acid salt and desorption by heat or mineralization, Chem. Eng. J. 405 (2021), 126938.

[16] B. Arias, M. Alonso, C. Abanades, CO_2 capture by calcium looping at relevant conditions for cement plants: experimental testing in a 30 kWth pilot plant, Ind. Eng. Chem. Res. 56 (10) (2017) 2634–2640.

[17] F.M. Brethomé, N.J. Williams, C.A. Seipp, M.K. Kidder, R. Custelcean, Direct air capture of CO_2 via aqueous-phase absorption and crystalline-phase release using concentrated solar power, Nat. Energy 3 (7) (2018) 553–559.

[18] R. Custelcean, N.J. Williams, K.A. Garrabrant, P. Agullo, F.M. Brethomé, H. J. Martin, M.K. Kidder, Direct air capture of CO_2 with aqueous amino acids and solid bis-iminoguanidines (BIGs), Ind. Eng. Chem. Res. 58 (51) (2019) 23338–23346.

[19] K.A. Garrabrant, N.J. Williams, E. Holguin, F.M. Brethomé, C. Tsouris, R. Custelcean, Energy-efficient CO_2 capture from flue gas by absorption with amino acids and crystallization with a bis-iminoguanidine, Ind. Eng. Chem. Res. 58 (24) (2019) 10510–10515.

[20] A.I. Papadopoulos, F. Tzirakis, I. Tsivintzelis, P. Seferlis, Phase-change solvents and processes for postcombustion CO_2 capture: a detailed review, Ind. Eng. Chem. Res. 58 (13) (2019) 5088–5111.

[21] S. Zhang, Y. Shen, L. Wang, J. Chen, Y. Lu, Phase change solvents for post-combustion CO_2 capture: Principle, advances, and challenges, Appl. Energy 239 (2019) 876–897.

[22] R. Custelcean, N.J. Williams, C.A. Seipp, Guanidine compounds for carbon dioxide capture, US patent number 10,583,387 (2020).

[23] N.J. Williams, C.A. Seipp, F.M. Brethomé, Y.-Z. Ma, A.S. Ivanov, V.S. Bryantsev, M. K. Kidder, H.J. Martin, E. Holguin, K.A. Garrabrant, R. Custelcean, CO_2 capture via crystalline hydrogen-bonded bicarbonate dimers, Chem 5 (3) (2019) 719–730.

[24] M. Kamali-Ardakani, H. Modarress, V. Taghikhani, M. Khoshkbarchi, Activity coefficients of glycine in aqueous electrolyte solutions: experimental data for (H_2O + KCl+ glycine) at T= 298.15 K and (H_2O+ NaCl+ glycine) atT= 308.15 K, J. Chem. Thermodyn. 33 (7) (2001) 821–836.

[25] J.T. Edsall, M.H. Blanchard, The activity ratio of zwitterions and uncharged molecules in ampholyte solutions. The dissociation constants of amino acid esters, J. Am. Chem. Soc. 55 (6) (1933) 2337–2353.

[26] H.-J. Song, S. Lee, K. Park, J. Lee, D. Chand Spah, J.-W. Park, T.P. Filburn, Simplified estimation of regeneration energy of 30 wt% sodium glycinate solution for carbon dioxide absorption, Ind. Eng. Chem. Res. 47 (24) (2008) 9925–9930.

[27] M. Castro, D. Gómez-Díaz, J.M. Navaza, A. Rumbo, Carbon dioxide capture by chemical solvents based on amino acids: absorption and regeneration, Chem. Eng. Technol. 44 (2) (2021) 248–257.

[28] H. Cai, X. Zhang, L. Lei, C. Xiao, Direct CO2 capture from air via crystallization with a trichelating iminoguanidine ligand, ACS Omega 5 (32) (2020) 20428–20437.

[29] L. Wang, Y. Zhang, R. Wang, Q. Li, S. Zhang, M. Li, J. Liu, B. Chen, Advanced monoethanolamine absorption using sulfolane as a phase splitter for CO2 capture, Environ. Sci. Technol. 52 (24) (2018) 14556–14563.

[30] Q. Ye, X. Wang, Y. Lu, Screening and evaluation of novel biphasic solvents for energy-efficient post-combustion CO2 capture, Int. J. Greenhouse Gas Control 39 (2015) 205–214.